Supporting Information

Accounting for Bifurcating Pathways in the Screening for CO_2 Reduction Catalysts

Federico Calle-Vallejo* and Marc T. M. Koper*

Leiden Institute of Chemistry, Leiden University, PO Box 9502, 2300 RA Leiden, The Netherlands.

*Correspondence to: F.C.-V.: f.calle.vallejo@chem.leidenuniv.nl,

M.T.M.K.: m.koper@chem.leidenuniv.nl

Table of contents

S1. Computational methods

The DFT calculations in this study were carried out with the VASP code.[1] We used the PBE exchange-correlation functional[2] to assess the exchange-correlation contributions to the total energy and the PAW method[3] to describe the ion-electron interactions. The geometry optimizations, made with a plane-wave cutoff of 450 eV, were performed with the conjugate gradient method, using 0.05 eV $Å^{-1}$ as convergence criterion for the maximal residual forces on every atom. The simulated slabs contained at least 4 atomic layers the two bottommost of which were fixed at the converged bulk interatomic distances, while the remaining layers and the adsorbates were free to move in all directions. At least 13 Å of vacuum were added in the z direction of all supercells and dipole corrections were also added to avoid electrostatic interactions between periodic images. The k-point samplings were 6×6×1, 6×6×1, 6×4×1, 4×5×1, and 4×4×1 for the 2×2 (111), 2×2 (100), 2×1 (211), 3×1 (211) kinked, and 3AD@3×3 (111) surfaces, respectively. Given their ferromagnetic properties, spin unrestricted calculations were made for Co and Ni, see Figure S1, and Co was simulated in its fcc phase to facilitate the comparison with the other metals. The Methfessel-Paxton method[4] was used to smear the Fermi level with k_BT = 0.2 eV and all energies extrapolated to T = 0 K. The gas-phase references for the adsorption energies were CO and H_2, which were simulated in boxes of 15 ×15 ×15 $Å^3$ with k_BT = 0.001 eV. All these conditions ensured convergence of adsorption energies within 0.05 eV. The free energies were approximated as: $G = E_{DFT} + ZPE - TS + E_{solvation}$. The zero-point energies (ZPE) of the gases and adsorbates, and the vibrational entropy (TS_{vib}) corrections for the adsorbates were calculated through the harmonic-oscillator approximation. For the adsorbates, the ZPE and TS_{vib} corrections at 298.15 K were evaluated on the (111), (100) and (211) facets of Cu, Ag and Ir. The averages of the nine values and their standard deviations appear in Table S1. The small standard deviations allow for the average values to be used for all metals and facets.

Table S1. ZPE and TS_{vib} at T = 298.15 K. AVG: average. STDEV: standard deviation. All values are in eV.

species	AVG ZPE	AVG TSvib	STDEV ZPE	STDEV TSvib
*CO	0.18	0.13	0.03	0.04
*COH	0.46	0.15	0.02	0.02
*CHO	0.46	0.14	0.03	0.03

The total TS corrections for CO and H_2 were taken as 0.61 and 0.40 eV at T = 298.15 K. The total energy of CO was corrected as described in ref.[5] and we used the computational hydrogen electrode to describe the energetics of protons and electrons.[6] Solvation contributions to the adsorption energies were accounted for using previously reported values, namely -0.10 eV for *CO and *CHO and -0.38 eV for *COH.[5, 7]

S2. Spin polarization effects on adsorption-energy scaling relations

Figure S1 contains the results of spin restricted (left) and spin unrestricted (right) calculations on the (111) facets of the ferromagnetic metals Co and Ni. As can be seen from the equations of the linear regressions, although there exist sizable differences between the individual adsorption energies, such differences are proportional and do not modify the trends significantly.

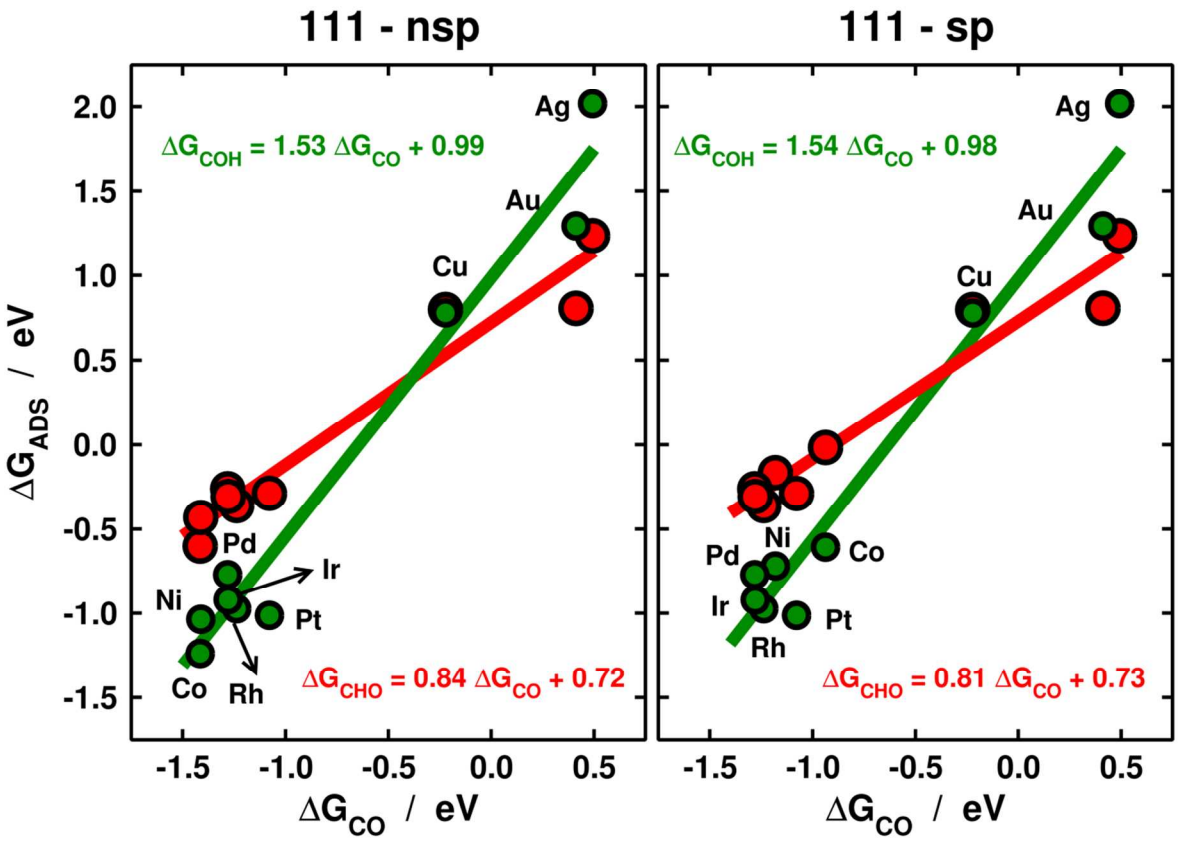

Figure S1. Spin-polarization effects on the scaling relations between the adsorption energies of *CO and *COH (green), and *CO and *CHO (red). The adsorption energies were calculated in the (111) facet. In each case the equations of the linear fits are provided. nsp: Spin restricted calculations, sp: spin restricted calculations.

S3. Origin of the unity slope for the scaling relationship of *CO vs. *CHO

It is well known that the slope of the scaling relation between the adsorption energies of *CO and *CHO is 1.[8-12] However, it is not straightforward to understand why, based on the electron-counting rules that typically determine the slope.[13-15] Take the case of *COH and *CO, the other adsorbates in this study. The C atom in *COH lacks three bonds to reach the octet, while the C atom in *CO lacks two, resulting in a slope of 3/2, as observed in Figures 2 and 3 in the main text. Along the same lines, the expected slope for *CHO vs *CO would be 1/2, as the C atom in *CHO lacks 1 bond to reach the octet. Then, how can then the unit slope be rationalized in simple terms?

First of all, it is important to note that in the vast majority of metals and sites considered here, *CHO is a bidentate adsorbate that binds to the surface through both C and O. The bond lengths in adsorbed *CHO are interesting, as they provide a simple way to understand the aforementioned unity slope. Figure S2 contains the metal-C, metal-O and C-O bond lengths of several adsorbates on Cu(111) and molecules in gas phase, calculated with DFT-PBE.

The C-Cu distance on Cu(111) for *CHO is 1.94 Å (Figure S2d), which is in between those of *CO (1.85 Å, Figure S2a) and $*CH_3$ (2.00 Å Figure S2b). Note that the C-Cu bond is double in *CO and single in $*CH_3$. This shows that the length of the C-Cu bond in *CHO is intermediate between a single and a double bond.

The length of the O-Cu bond in $*OCH_3$ is 1.87 Å (Figure S2c) and 1.86 Å in *OH (not shown). In those two cases, the O-Cu bond is single. In addition, the O-Cu distance in *CHO is 2.24 Å (Figure S2d). This shows that the length of the O-Cu bond in *CHO is considerably larger than that of a single bond.

The C-O bond length is 1.14 Å in CO(g) (C-O double bond plus a dative bond), 1.18 Å in *CO, 1.21 Å in CH_2O(g) (C-O double bond), 1.42 Å in $*OCH_3$ (C-O single bond) and 1.43 Å in CH_3OH(g) (C-O single bond). The C-O distance of 1.25 Å in *CHO is, therefore, intermediate between those of double and single C-O oxygen bonds.

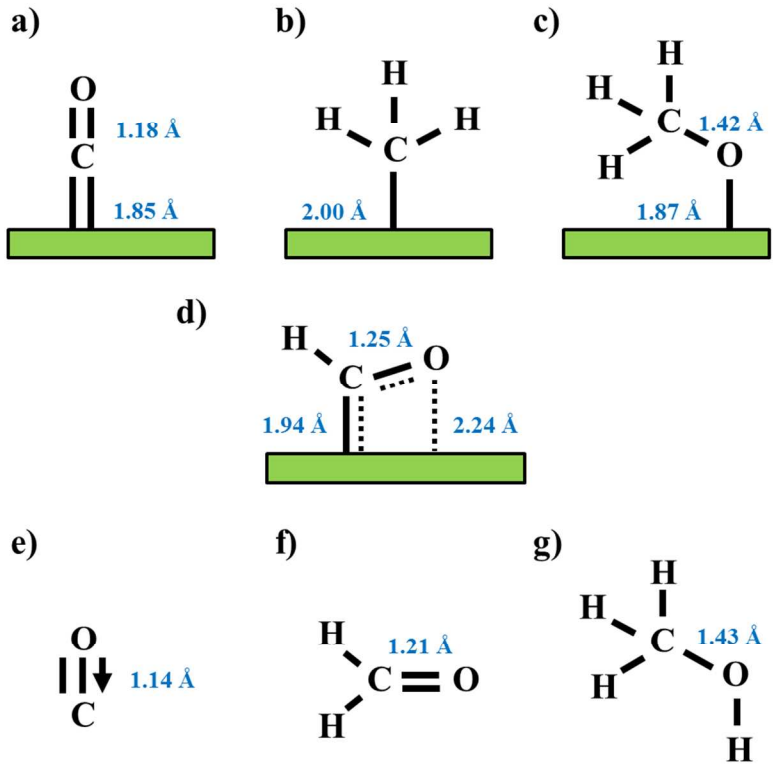

Figure S2. C-O, C-Cu and O-C bond lengths in various adsorbates on Cu(111) and molecules of interest. a) Adsorbed CO, where there is a double C-Cu bond. b) Adsorbed methyl, where there is a single C-Cu bond. c) Adsorbed methoxy, where there is a single O-Cu bond. In a)-c) the adsorption site is atop. d) Adsorbed CHO adsorbed in a bidentate configuration. e) Carbon monoxide, where there is a C-O double bond and a dative bond. f) Formaldehyde, where there is a C-O double bond. g) Methanol, where there is a single C-O bond.

In summary, the C-Cu and C-O distances in *CHO are intermediate between those characteristic of single and double bonds. On the other hand, the O-Cu distance in *CHO is considerably larger than a typical O-Cu single bond. Bearing in mind that bond lengths and bond strengths are inversely correlated (shorter bond distances imply stronger bonds), we conclude that the C-Cu and C-O bonds in *CHO are more than single but less than double and that the O-Cu bond is less than a single bond. To conclude, although the valence of CHO(g) is 1, that of *CHO is more than 1 in view of its bidentate adsorption configuration. The fact that the observed slopes in Figures 2 and 3 are close to 1 reveals that the bond between *CHO and a metal surface is double and the adsorbed valence of *CHO is larger than that of CHO(g).

S4. Solvation effects on pathway bifurcation

While the main text contains the initial results (*CO/*CHO/*COH solvation corrections of -0.1/-0.1/-0.38 eV) two more cases are considered in this section: I) a hypothetical case in which solvation is identical for *CO, *CHO and *COH (any value renders the same results), which largely favors *CHO formation and makes U_L more negative with respect to the initial results, as shown in Table S2 and Figure S3.

Table S2. Most stable adsorbates formed upon the *CO hydrogenation with identical *CO/*CHO/*COH solvation corrections. In case $abs(\Delta G_{COH} - \Delta G_{CHO}) < 0.1$ eV , both intermediates are reported.

metal	111, cn =9	100, cn = 8	211, cn = 7	211k, cn = 6	3AD@111, cn = 5
Co	COH	CHO	both	both	CHO
Rh	COH	both	both	CHO	CHO
Ir	COH	COH	both	CHO	CHO
Ni	COH	both	both	both	CHO
Pd	COH	COH	both	both	both
Pt	COH	COH	both	both	CHO
Cu	CHO	CHO	CHO	CHO	CHO
Ag	CHO	CHO	CHO	CHO	CHO
Au	CHO	CHO	CHO	CHO	CHO

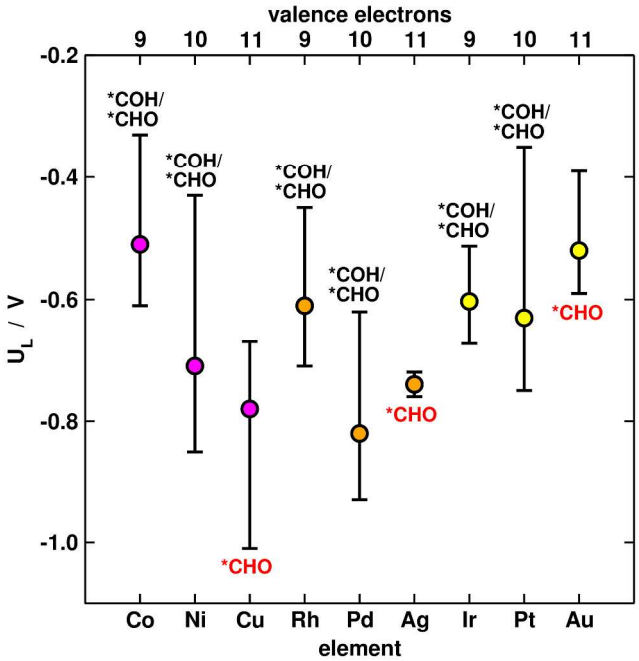

Figure S3. *CO hydrogenation potentials when *CO, *CHO, *COH are identically solvated.

II) A case in which *COH has a solvation correction of -0.5 eV while those of *CHO and *CO stays at -0.1 eV, which favors *COH formation and makes U_L less negative compared to the initial results, as show below:

Table S3. Most stable adsorbates formed upon *CO hydrogenation with *CO/*CHO/*COH solvation corrections of -0.1/-0.1/-0.5 eV. In case $abs(\Delta G_{COH} - \Delta G_{CHO}) < 0.1$ eV , both intermediates are reported.

metal	111 cn =9	100 cn = 8	211 cn = 7	211k cn = 6	3AD@111 cn = 5
Co	COH	COH	COH	COH	both
Rh	COH	COH	COH	COH	COH
Ir	COH	COH	COH	COH	COH
Ni	COH	COH	COH	COH	COH
Pd	COH	COH	COH	COH	COH
Pt	COH	COH	COH	COH	COH
Cu	COH	COH	CHO	CHO	CHO
Ag	CHO	CHO	CHO	CHO	CHO
Au	CHO	CHO	CHO	CHO	CHO

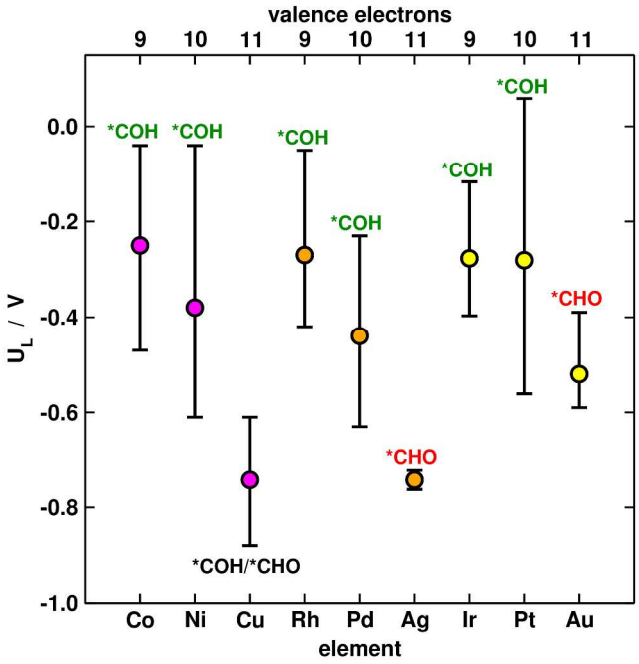

Figure S4. *CO hydrogenation potentials with *CO/*CHO/*COH solvation corrections of -0.1/-0.1/-0.5 eV.

REFERENCES

1. Kresse, G.; Furthmüller, J. *Phys. Rev. B* **1996,** *54*, 11169-11186.

2. Perdew, J. P.; Burke, K.; Ernzerhof, M. *Phys. Rev. Lett.* **1997,** *78*, 1396-1396.

3. Kresse, G.; Joubert, D. *Phys. Rev. B* **1999,** *59*, 1758-1775.

4. Methfessel, M.; Paxton, A. T. *Phys. Rev. B* **1989,** *40*, 3616-3621.

5. Calle-Vallejo, F.; Koper, M. T. M. *Angew. Chem. Int. Ed.* **2013,** *52*, 7282-7285.

6. Nørskov, J. K.; Rossmeisl, J.; Logadottir, A.; Lindqvist, L.; Kitchin, J. R.; Bligaard, T.; Jónsson, H. *J. Phys. Chem. B* **2004,** *108*, 17886-17892.

7. Peterson, A. A.; Abild-Pedersen, F.; Studt, F.; Rossmeisl, J.; Norskov, J. K. *Energy Environ. Sci.* **2010,** *3*, 1311-1315.

8. Hansen, H. A.; Shi, C.; Lausche, A. C.; Peterson, A. A.; Norskov, J. K. *Phys. Chem. Chem. Phys.* **2016,** *18*, 9194-9201.

9. Hansen, H. A.; Varley, J. B.; Peterson, A. A.; Nørskov, J. K. *J. Phys. Chem. Lett.* **2013,** *4*, 388-392.

10. Jovanov, Z. P.; Hansen, H. A.; Varela, A. S.; Malacrida, P.; Peterson, A. A.; Nørskov, J. K.; Stephens, I. E. L.; Chorkendorff, I. *J. Catal.* **2016,** *343*, 215-231.

11. Peterson, A.; Grabow, L.; Brennan, T.; Shong, B.; Ooi, C.; Wu, D.; Li, C.; Kushwaha, A.; Medford, A.; Mbuga, F.; Li, L.; Nørskov, J. *Top. Catal.* **2012,** *55*, 1276-1282.

12. Peterson, A. A.; Nørskov, J. K. *J. Phys. Chem. Lett.* **2012,** *3*, 251-258.

13. Abild-Pedersen, F.; Greeley, J.; Studt, F.; Rossmeisl, J.; Munter, T. R.; Moses, P. G.; Skúlason, E.; Bligaard, T.; Nørskov, J. K. *Phys. Rev. Lett.* **2007,** *99*, 016105.

14. Calle-Vallejo, F.; Loffreda, D.; Koper, M. T. M.; Sautet, P. *Nat. Chem.* **2015,** *7*, 403-410.

15. Calle-Vallejo, F.; Martinez, J. I.; Garcia-Lastra, J. M.; Rossmeisl, J.; Koper, M. T. M. *Phys. Rev. Lett.* **2012,** *108*.